High efficiency and low threshold current strained V-groove quantum-wire lasers

Sandip Tiwari, G. David Pettit, Keith R. Milkove, and Francoise Legoues
IBM Research Division, Thomas J. Watson Research Center, Yorktown Heights, New York 10598

Robert J. Davis
Department of Electrical Engineering, Columbia University, New York, New York 10027

Jerry M. Woodall
Department of Electrical Engineering, Purdue University, West Lafayette, Indiana 47907

(Received 10 March 1994; accepted for publication 13 April 1994)

Multi-quantum-wire strained lasers are reported in the $Ga_{1-x}In_xAs/Ga_{1-x}Al_xAs$ semiconductor material system with a minimum threshold current of 188 μA and maximum powers of $\approx$50 μW in continuous multimode operation at wavelengths of $\approx$980 nm and differential output of $\approx$0.5 μW/μA. The structures, fabricated by molecular-beam epitaxy, are self-aligned, self-isolated, and minimize electrical and optical losses. Internal quantum efficiencies are $\approx$83% and internal losses are $\approx$4.2 cm^{-1}. Characteristic temperatures of $\approx$260 K, and an increase in threshold current and lasing wavelength under externally applied stress changing from compressive to tensile conditions, show that the major determinants of lasing threshold are density of states and optical losses.

Quantum-wire lasers, fabricated by metalorganic chemical vapor deposition in the $GaAs/Ga_{1-x}Al_xAs$ system[1–3] have exhibited spectral characteristics that have been expected in this reduced-dimension system. An important advantage of the quantum-wire lasers is the expected reduction in threshold current due to scaling of active volume as well as due to increase in differential gain by multidimensional confinement. Here, we report reduction in threshold current to sub -200 μA and other related properties.

Figures 1(a) and 1(b) show schematic cross section of the grown structure together with a secondary electron micrograph. A silicon nitride mask is used to form a V-shaped groove for the growth with the cavity in $\langle 01\bar{1} \rangle$ orientation. Electronic devices[4] and optical devices[5] have successfully utilized dielectric masking in crystalline active growth, but resulted in an interface between the polycrystalline material that grows on the dielectric layer and the single-crystal material. In unipolar electronic devices, this causes depletion of carriers at the boundaries and anomalous diffusion. In bipolar devices, this also adds excess carrier recombination. In the structures grown, these effects are entirely avoided by the choice of a large undercut commensurate with the design of the gain-guiding region within optical and electronic constraints. More significantly, in molecular beam epitaxy, like metalorganic vapor deposition,[6] the adatom migration properties of aluminum, gallium, and indium on different surfaces can be employed to obtain a structure where the quantum wells can be enclosed within the cladding region, and where the growth rate changes on different planes can be utilized to significantly decrease the well thickness along the walls and to increase it at the bottom, where (100) planes appear preferentially. Some of these attributes are visible in Fig. 1(a), which shows the last to grow $Ga_{1-x}Al_xAs$ cladding and GaAs contact regions extending significantly further than the opening in the mask. The V grooves are etched to reveal planes that are slightly off-axis from (111). The surface mobility of the adatoms appears to be in the order Ga>Al>In during growth. The higher growth rates of (100) plane at the bottom of the groove, and of (311) plane elsewhere, is an important consequence of the growth process.

Thus $Ga_{1-x}In_xAs$ quantum wires result at the bottom of the growth groove. Thinner quantum wells occur along the wall with a severe necking of the quantum wire and the entire $Ga_{1-x}In_xAs$ region is clad with $Ga_{1-x}Al_xAs$ and GaAs. The structures utilize three quantum wires to enhance gain; on (100) planar surface, grown simultaneously, the wells are 80 Å in thickness and displaced by 40 Å of GaAs with 20 Å of GaAs at the bottom and top before the linear grading of $Ga_{1-x}Al_xAs$. Cross-sectional transmission electron micrographs reveal actual wire thicknesses of 100–115 Å, approximately crescent in shape, with the larger thicknesses and smaller lateral spreading occurring at the bottom. The structure is composed of a bottom n-type contact layer on n^+ substrate, a $Ga_{0.25}Al_{0.75}As$ cladding layer, a graded 1000-Å $Ga_{1-x}Al_xAs$ layer, triple quantum wells of nominally $Ga_{0.8}In_{0.2}As$ composition with GaAs barrier regions, followed by a p-type graded, cladding, and contact layers which have similar thicknesses as the n-type regions. The choice of high AlAs mole fraction and thin graded region was strictly to enhance the optical confinement factor of the structure which is estimated to be 0.016. Polycrystalline material has a resistivity exceeding 10^6 Ω cm; the devices are isolated from each other as a result of the growth and require a thick contact metallurgy that can be directly evaporated following a single lithographic step to open top contact holes.

Figure 2 shows 300-K light output characteristics of the lowest threshold current (188-μA) laser measured. The figure also shows the spectral output at three different bias currents. The laser is 1 mm long and employs no facet coating. It exhibits a peak output power of $\approx$50 μW. At a reverse bias of 2 V, these lasers typically exhibit a leakage current less than 2 μA and in the forward bias range of 0.3–0.7 V, have an ideality of $\approx$1.3. These are indicative of the very low

 0003-6951/94/64(26)/3536/3/$6.00

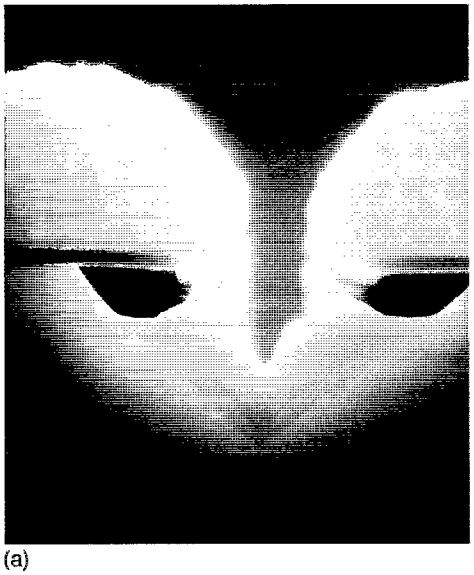

(a)

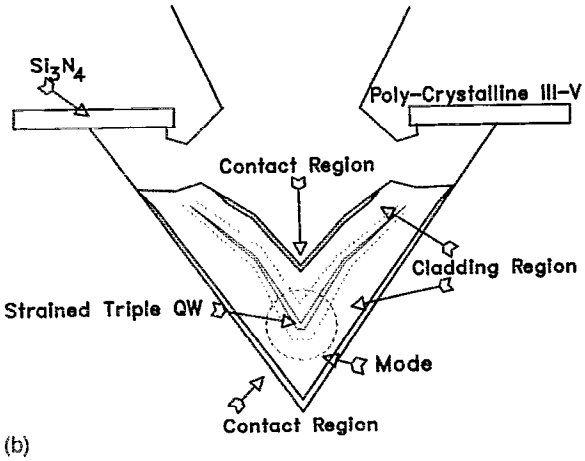

(b)

FIG. 1. (a). Scanning electron micrograph of a V-groove cross section, following fabrication of the laser structure. (b) shows a schematic cross section identifying various regions and pointing out effects related to growth. In (a), the nitride opening is 5 μm.

parasitic nonradiative generation-recombination current at the surfaces, where the junctions now occur in larger band gap material of GaAs and $Ga_{1-x}Al_xAs$. Another attribute of the grown structure is low current along the sloped wall because of thinner wells, smaller InAs mole fraction in the wells, and necking of the quantum wires.

The optical confinement in these structures is similar in both the vertical and the horizontal direction because the walls are sloped at $\approx$45°. From the inverse quantum efficiency plot of Fig. 3, which shows averaged data from five devices in close proximity, the internal quantum efficiency (η_i) is estimated to be 0.834, and the internal loss, α_i, to be 4.21 cm^{-1}. The figure also shows a similar plot for ridge lasers, 1.5 μm in width and 1 mm in length, grown simultaneously. η_i is quite typical of commonly reported values of quantum-well ridge lasers, although the best reports have approached unity. α_i, however, is significantly improved over the best reported values of $\approx$6–9 cm^{-1}. The internal losses are a factor of 3 smaller than mirror loss for 1-mm

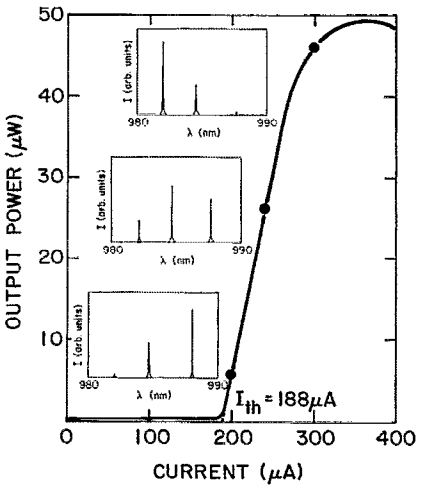

FIG. 2. Light power-current characteristics and spectra at different biases for the minimum threshold current laser measured.

length without the use of mirror coatings. Therefore, with the use of mirror coatings, it should be possible to reduce the threshold current even further. The low losses also indicate success in use of large mole fraction of AlAs. The high η_i shows that, at the least, nonradiative losses are scaled as the radiative cross section has been scaled.

The far-field patterns are approximately circularly symmetric with a full width at half-maximum of 20°, reinforcing the basis of the operation of these lasers in two-dimensional index confinement. Light is polarized in the transverse electric field (TE) mode in the plane of substrate, i.e., gain of TE mode determined from the characteristics of the lateral potential well determine the characteristics of the emitted radiation. Absence of kinks in output light-current characteristics shows that only a single mode is excited. In Fig. 2, blue

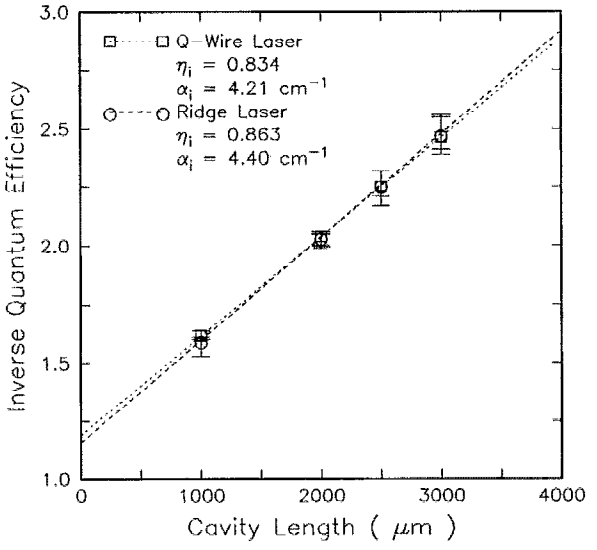

FIG. 3. Inverse of efficiency as a function of cavity length. The data points are averages for five lasers measured in close proximity of each other on the wafer.

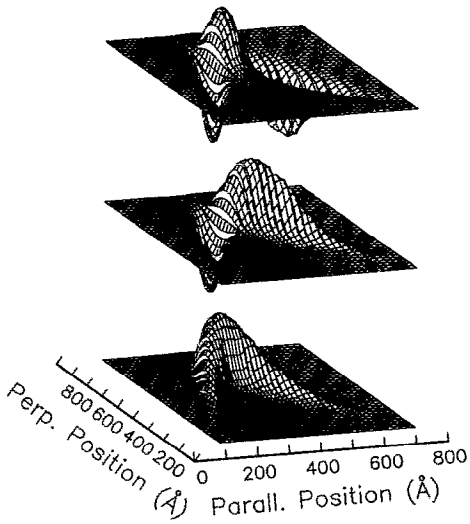

FIG. 4. Envelope functions for electrons in a crescent-shaped well of a single $Ga_{0.8}In_{0.2}As$ well in a GaAs and $Ga_{1-x}Al_xAs$ matrix which approximates the structures grown for one well and ignores the grading region. The energy-level solutions are determined by the lateral confinement and indicate subband energies 3–4 meV apart.

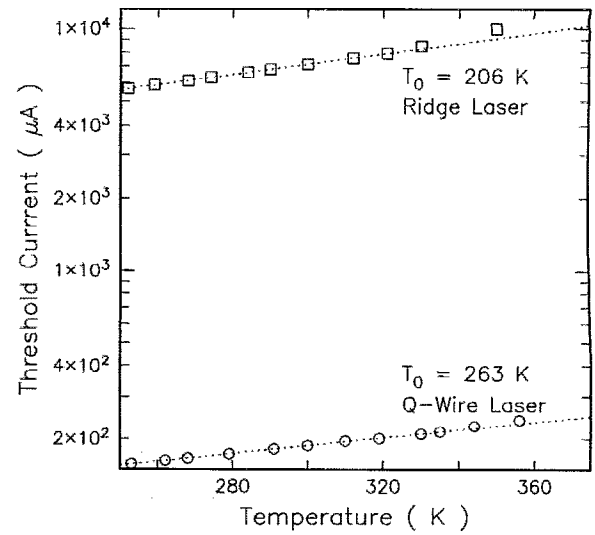

FIG. 5. Threshold current as a function of operating temperature for quantum-wire and ridge lasers fabricated from material grown simultaneously. Both lasers are 1 mm long, and the ridge lasers are 1.5 μm in width.

shifting of radiated lines is observed as a consequence of larger drive current. This shifting of 4–5 meV is similar to that reported by Simhony *et al.*[2] and is caused by occupation of higher order subbands of the quantum wires. Estimates have been made using a Schrödinger–Poisson solver[7,8] by approximating the shape observed in transmission-electron micrographs to a single crescent-shaped quantum wire of $Ga_{0.8}In_{0.2}As$ in order to estimate the approximate electron energy level spacing. These calculations (see Fig. 4 for envelope functions) confirm expected electron energy-level spacings of 3–4 meV, slightly smaller than measured spacings which also include effects of hole energy subbands. The lateral spread of the quantum wires is the important confining dimension.

These observations all reinforce the optimization of the design, growth, and operation of these quantum-wire lasers. Electrical and optical losses have been minimized and differential gain improved by using three strained quantum wires and large and rapid index changes that enhance optical confinement factor and band-edge valence band density-of-states. Measurements of lasers across an inch-wide region indicate sufficient variations (Fig. 3 also indicates larger variations at longer cavity lengths) that come about due to inhomogeneity effects as a consequence of well-width variations in the growth direction and longitudinally along the cavity, as well as due to initial variations in depth of the V groove. The operation at distinct energies indicates that this is still a sub-1% length effect in any 1-mm-long region.

Strain is significant to the lowering of the threshold current. Uniaxially applied external stress causes the threshold current to decrease during a compressive in-plane strain and it causes the threshold current to increase during a tensile in-plane strain. The threshold current decreases by 15%–20% for a 0.1% in-plane compressive strain. This behavior, similar to that of quantum-well strained lasers,[9] confirms that Auger recombination effects, or other small band gap recombination effects, do not determine the operation of this laser. Figure 5 shows the characteristic temperature of quantum-wire and 1.5-μm-wide ridge lasers, both 1 mm in length. An improvement of $\approx$30% is observed. This is significant, but considerably less than predicted improvements for quantum-wire structures.[10] Carrier heating in the presence of reduced density of states, comparable stimulated emission and inter- and intra-band relaxation, and breakdown of selection rule in the presence of inhomogeneities are possible causes for this.

The authors thank Steve Laux, Arvind Kumar, and Frank Stern for help in use of SCRAPS—a three-dimensional Poisson–Schrödinger solver, and for development of the program.

[1] E. Kapon, J. P. Harbison, C. P. Yun, and N. G. Stoffel, Appl Phys. Lett. **54**, 304 (1989).
[2] S. Simhony, E. Kapon, E. Colas, D. M. Hwang, N. G. Stoffel, and P. Worland, Appl. Phys. Lett. **59**, 2225 (1991).
[3] M. Walther, E. Kapon, E. Colas, D. M. Hwang, and R. Bhat, Appl. Phys. Lett. **60**, 521 (1991).
[4] G. M. Metze, H. M. Levy, D. W. Woodard, C. E. C. Wood, and L. F. Eastman, Appl. Phys. Lett. **37**, 628 (1980).
[5] J. M. Hong, M. C. Wu, S. Wang, W. I. Wang, and L. L. Chang, Appl. Phys. Lett. **60**, 413 (1992).
[6] R. Bhat, E. Kapon, S. Simhony, E. Colas, D. M. Hwang, N. G. Stoffel, and M. A. Koza, J. Cryst. Growth **107**, 716 (1991).
[7] S. E. Laux and F. A. Stern, Appl. Phys. Lett. **49**, 91 (1986).
[8] A. Kumar, S. E. Laux, and F. A. Stern, Phys. Rev. B **42**, 5166 (1990).
[9] S. Tiwari, R. S. Bates, C. S. Harder, and A. Behfar-Rad, Appl. Phys. Lett. **60**, 413 (1992).
[10] Y. Arakawa and H. Sakaki, Appl. Phys. Lett. **40**, 939 (1982).